

复杂相贯线接缝自动焊接的运动控制算法

霍孟友，岳少剑，王新刚
(山东大学 机械工程学院, 济南 250061)



霍孟友

摘 要: 为了实现复杂相贯线接缝的自动焊接, 在简要介绍设计的五轴联动数控焊接机床组成结构与工作原理的基础上, 以椭球面封头自动焊接接管为例, 重点介绍了通过坐标变换构建相贯线接缝曲线方程, 再以相同的参数角 φ 将相贯线接缝曲线离散化成 N 段首尾相接的小直线段, 利用小直线段插补拟合整条相贯线接缝曲线, 给出了各插补离散点坐标参数与焊枪姿态调整的计算方法, 最后采用通用数字 I/O 卡和步进电机构成伺服控制系统执行运动控制算法。文中介绍的这种运动控制算法, 具有较高的通用性, 并且大幅度地降低了设备成本。

关键词: 自动焊接; 相贯线接缝; 伺服控制算法

中图分类号: TP273 文献标识码: A 文章编号: 0253-360X(2006)12-009-04

0 序 言

由于管与管之间、锅炉封头与接管之间等连通焊接的相贯线接缝较为复杂, 故一般采用自动焊接以满足较高的焊接质量和效率要求。根据焊接工艺, 在自动焊接过程中焊枪的轴线应与形成相贯线的两实体表面之间保持一定的夹角, 因此, 焊枪除了要求具备平动功能外, 还需要对其进行姿态控制, 这样才能使焊枪在允许的误差范围内准确跟踪相贯线接缝, 并通过控制焊枪姿态来保证接缝的焊接质量。因此, 对焊枪至少需要五个自由度(x, y, z, A, B)的位置和姿态联合控制才能够满足复杂相贯线接缝的自动焊接运动控制要求。

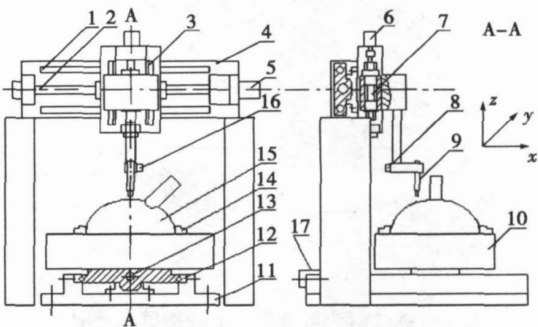
目前, 针对复杂相贯线接缝焊接的伺服运动控制技术研究很少, 而已有的数控焊接机床^[1,2]存在功能单一以及通用性较低的技术缺陷; 为了完成多自由度的联动过程控制, 很多设备往往选用成本较高的多轴运动伺服控制卡(如 PMAC), 依托硬件完成复杂算法的处理, 大大增加了设备成本。

考虑到实际焊接速度较慢而计算机处理速度非常高的基本情况, 根据文中设计的五个自由度数控焊接机床, 以椭球面封头焊接接管为例, 详细介绍了相贯线接缝空间曲线方程的构建、利用直线段插补拟合接缝曲线时各插补离散点坐标参数计算与焊枪

姿态调整, 以及采用通用数字 I/O 卡和步进电机构成伺服控制系统的实现方法。这种基于软件的数控系统思想设计的焊接运动控制算法可以大大地降低设备的成本^[3], 故具有较大的性价比优势。

1 焊接机床结构及工作原理

图 1 是设计的五轴联动自动焊接机床的组成结构示意图。它利用 y 向电机和 z 向电机实现焊枪移动控制, 利用 x 向电机完成焊接件移动控制, 而利



1 y 向导轨; 2 y 向滚珠丝杠; 3 z 向导轨; 4 横梁;
5 y 向电机; 6 z 向电机; 7 z 向丝杠; 8 A 轴电机;
9 焊枪; 10 工作台; 11 底座; 12 x 向导轨; 13 x 向丝杠;
14 夹具; 15 焊接件; 16 B 轴电机; 17 x 向电机

图 1 自动焊接机床结构示意图

Fig 1 Schematic diagram of automatic welding machine structure

用 A, B 轴电机完成焊枪姿态控制调整, 通过运动合成完成复杂相贯线接缝的自动焊接运动控制。

五个电机均选用可以细分驱动的混合式步进电机, 以降低设备成本。步进电机由驱动器驱动控制, 而驱动器通过插接在 PCI 插槽中廉价的通用 I/O 板卡控制各步进电机运转的方向和速度。

2 焊接运动控制算法

完成复杂相贯线接缝的自动焊接, 需要焊接轨迹跟踪运行控制, 所以首先需要构建相贯线接缝的数学模型。在建立了相贯线接缝数学模型以后, 再以相同的参数角 φ_s ($\varphi_s = 2\pi/N$) 将连续的相贯线接缝离散化成 N 小段, 形成 N 个离散点 P_i ($i=1, 2, \dots, N$) (第 i 个离散点对应的参数角为 $\varphi_i = i\varphi_s$), 然后以直线段连接每两个相邻的离散点, 用这 N 段首尾相接的小直线段插补拟合整条空间曲线。只要 φ_s 取值足够小, 插补轨迹就能够满足给定的误差要求, 使焊接轨迹处于要求的误差精度范围内^[4]。

这里以椭球面封头焊接接管(如锅炉封头焊接接管)为例说明实现复杂相贯线接缝自动焊接的运动控制算法。

2.1 相贯线参数方程

图 2 是椭球面封头与接管的相贯线接缝示意图。

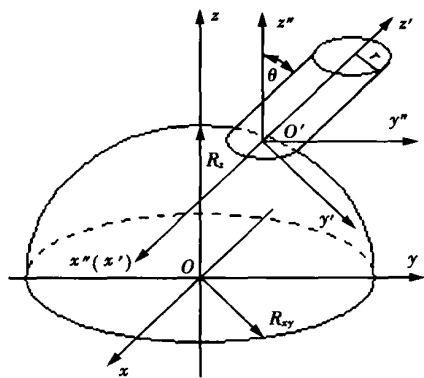


图 2 锅炉封头与接管相贯线接缝示意图

Fig 2 Schematic diagram of intersection seam of boiler end and conjugation tube

以接管轴线与椭球球心 O 确定的平面为 yOz 平面建立右手笛卡尔坐标系 $Oxyz$, 设接管轴线与椭球面的交点记为 $O'(a, b, c)$ 。将坐标系平移至 O' 点, 形成了辅助坐标系 $O'x'y'z'$; 再把 $O'x'y'z'$ 坐标

系以 $O'x''$ 为轴线旋转角度, 使 $O'z''$ 轴旋转至接管的轴线位置即变成了辅助坐标系, 这里 $O'x'$ 与 $O'x''$ 同轴。设椭球面在 xOy 平面内的半径为 R_y , 在 Oz 坐标轴方向的半径为 R_z ; 接管半径为 r , 且 $R_y > r, R_z > r$, 则椭球面封头在坐标系中的方程为

$$\frac{x^2 + y^2}{R_y^2} + \frac{z^2}{R_z^2} = 1. \quad (1)$$

而圆柱接管在 $O'x'y'z'$ 坐标系中的方程为

$$x'^2 + y'^2 = r'^2. \quad (2)$$

由解析几何可知, 坐标系 $Oxyz$ 和 $O'x'y'z'$ 之间存在如下坐标变换关系

$$\begin{bmatrix} x \\ y' \\ z' \end{bmatrix} = \begin{bmatrix} 1 & 0 & 0 \\ 0 & \cos \theta & -\sin \theta \\ 0 & \sin \theta & \cos \theta \end{bmatrix} \cdot \begin{bmatrix} x-a \\ y-b \\ z-c \end{bmatrix}. \quad (3)$$

从而在 $Oxyz$ 坐标系中圆柱接管的方程变为

$$(x-a)^2 + [(y-b)\cos \theta - (z-c)\sin \theta]^2 = r'^2. \quad (4)$$

由式(1), (4)求得相贯线接缝的参数方程为

$$\begin{cases} x = r \cos \varphi + a, \\ y = \frac{R_y}{P} [R_z \sin \theta \sqrt{l_2 P - l_1^2} + l_1 R_{xy} \cos \theta], \\ z = \frac{R_z}{P} [R_y \cos \theta \sqrt{l_2 P - l_1^2} - l_1 R_z \sin \theta]. \end{cases} \quad (5)$$

式中: $P = R_y^2 \cos^2 \theta + R_z^2 \sin^2 \theta$;

$$l_1 = r \sin \varphi + b \cos \theta - c \sin \theta;$$

$$l_2 = 1 - \frac{(r \cos \varphi + a)^2}{R_y^2}.$$

φ 为相贯线坐标点 (x', y', z') 在 $x'O'y'$ 平面中与 $O'x'$ 轴的夹角, 取值范围为 $[0, 2\pi]$ 。

2.2 离散点坐标参数计算

焊枪末端在离散点 $P_i(x_i, y_i, z_i)$ 处时, 焊枪的姿态应满足: (1) 焊枪应位于相贯线接缝在离散点 P_i 处的法平面内; (2) 焊枪应处于法平面与两空间曲面交线的角平分线上。

由相贯线参数方程可得, 接缝上某离散点 $P_i(x_i, y_i, z_i)$ 处的法平面方程为

$$\begin{aligned} x'(\varphi_i)(x-x_i) + y'(\varphi_i)(y-y_i) + \\ z'(\varphi_i)(z-z_i) = 0, \end{aligned} \quad (6)$$

$$\text{可简化为 } A_1 x + A_2 y + A_3 z + A_4 = 0, \quad (7)$$

式中: A_1, A_2, A_3, A_4 均为常数。

由式(4), (7)可得法平面与圆柱接管的交线在离散点 $P_i(x_i, y_i, z_i)$ 处的切向量 τ_1 为

$$\begin{cases} x_1' = -r \sin \varphi_i, \\ y_1' = \frac{A_1 r \sin \theta \sin \varphi_i + A_3 r \cos \varphi_i}{A_3 \cos \theta + A_2 \sin \theta}, \\ z_1' = \frac{A_1 r \cos \theta \sin \varphi_i - A_2 r \cos \varphi_i}{A_3 \cos \theta + A_2 \sin \theta}. \end{cases}$$

同理, 由式(1), (7)可求得法平面与椭球面交线在点 $P_i(x_i, y_i, z_i)$ 处的切向量 τ_2 为

$$\begin{cases} x_2' = -r \sin \varphi_i, \\ y_2' = \frac{R_{xy}}{Q} (|A_3| R_z F + A_1 A_2 R_{xy} r \sin \varphi_i), \\ z_2' = \frac{R_z}{Q} (|A_2| R_{xy} F + A_1 A_3 R_z r \sin \varphi_i). \end{cases}$$

式中: $Q = A_2^2 R_{xy}^2 + A_3^2 R_z^2$;

$$F = \frac{r \sin \varphi_i (r \cos \varphi_i + a) Q - A_1 l_3(\varphi_i) R_{xy}^2 r \sin \varphi_i}{R_{xy}^2 \sqrt{l_2(\varphi_i) Q - l_3^2(\varphi_i)}}.$$

将切向量 τ_1 和切向量 τ_2 分别单位化得到 $\eta_1 = \{x_1, y_1, z_1\}$, $\eta_2 = \{x_2, y_2, z_2\}$, 则焊枪矢量为 $\eta = \{x_1 + x_2, y_1 + y_2, z_1 + z_2\}$, 显然该矢量位于向量 τ_1 和 τ_2 的角平分线上。由此可得, 接缝上第 i 个离散点 $P_i(x_i, y_i, z_i)$ 处焊枪与 x, y 轴的夹角 A_i, B_i 分别为

$$A_i = \arccos \frac{x_1 + x_2}{\sqrt{(x_1 + x_2)^2 + (y_1 + y_2)^2 + (z_1 + z_2)^2}},$$

$$B_i = \arccos \frac{y_1 + y_2}{\sqrt{(x_1 + x_2)^2 + (y_1 + y_2)^2 + (z_1 + z_2)^2}}.$$

依此类推, 可以得到相贯线上所有其它离散点的五个坐标值, 即 x_i, y_i, z_i, A_i, B_i 。

2.3 插补计算

插补计算的目的是根据已知的离散点的坐标值求出每两个相邻的离散点之间所对应的五个运动自由度的位移量。图 3 是以椭圆封头接管焊接为例的运动控制插补计算示意图。

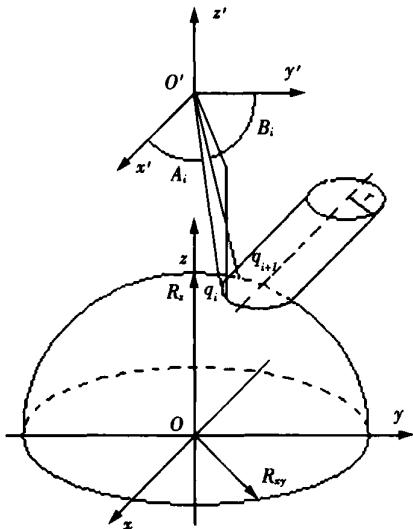


图 3 插补计算示意图

Fig. 3 Schematic diagram of interpolation algorithm

在图 3 中, 以焊枪顶端为原点建立焊枪坐标系 $O'x'y'z'$, 三个坐标轴的方向分别平行于工件坐标系 $Oxyz$ 的 x, y, z 轴, 则两坐标系中焊枪姿态 (A, B) 相同。在焊枪坐标系中, 设两个相邻离散点为 $P_i(x_i, y_i, z_i, A_i, B_i)$, $P_{i+1}(x_{i+1}, y_{i+1}, z_{i+1}, A_{i+1}, B_{i+1})$, 两点上焊枪位置矢量分别为 $q_i(a_i, b_i, c_i)$, $q_{i+1}(a_{i+1}, b_{i+1}, c_{i+1})$ 。设焊枪长度为 l , 在实际焊接过程中焊枪应位于 $x'O'y'$ 下, 由空间解析几何可知

$$\begin{cases} a_i = l \cos A_i, \\ b_i = l \cos B_i, \\ c_i = -l \sqrt{1 - \cos^2 A_i - \cos^2 B_i}. \end{cases} \quad (8)$$

$$\begin{cases} a_{i+1} = l \cos A_{i+1}, \\ b_{i+1} = l \cos B_{i+1}, \\ c_{i+1} = -l \sqrt{1 - \cos^2 A_{i+1} - \cos^2 B_{i+1}}. \end{cases} \quad (9)$$

由于焊接过程中需要焊枪绕自身坐标系的 x' 轴和 y' 轴旋转进行姿态调整, 那么焊枪末端就会偏离相贯线上的指定点一个向量, 即 $\{a_{i+1} - a_i, b_{i+1} - b_i, c_{i+1} - c_i\}$, 这时焊枪与工作台在一个插补周期中沿 x, y, z 轴移动的位移量将变为

$$\Delta x_i = x_{i+1} - x_i - l \cos A_{i+1} + l \cos A_i,$$

$$\Delta y_i = y_{i+1} - y_i - l \cos B_{i+1} + l \cos B_i,$$

$$\Delta z_i = z_{i+1} + l \sqrt{1 - \cos^2 A_{i+1} - \cos^2 B_{i+1}} - z_i - l \sqrt{1 - \cos^2 A_i - \cos^2 B_i}.$$

焊枪从 P_i 点移动到 P_{i+1} 点需要调整焊枪姿态的两个旋转自由度的位移量可利用以下方法求解。

矢量绕 x 轴和 y 轴旋转的旋转矩阵分别为

$$R(x, \alpha) = \begin{bmatrix} 1 & 0 & 0 \\ 0 & \cos \alpha & -\sin \alpha \\ 0 & \sin \alpha & \cos \alpha \end{bmatrix},$$

$$R(y, \beta) = \begin{bmatrix} \cos \beta & 0 & \sin \beta \\ 0 & 1 & 0 \\ -\sin \beta & 0 & \cos \beta \end{bmatrix}.$$

设 q_i 先绕 x 轴旋转 α , 后绕 y 轴旋转 β 得到 q_{i+1} , 则有

$$q_{i+1} = R(y, \beta) \circ R(x, \alpha) \circ q_i. \quad (10)$$

由(9)(10)两式联立求解可得两个旋转轴的位移量分别为

$$\alpha_i = \arcsin \frac{\cos B_{i+1}}{|\sin A_i|} - \arcsin \frac{\cos B_i}{|\sin A_i|},$$

$$\beta_i = \arcsin \frac{\cos A_{i+1}}{\sqrt{1 - \sin^2 A_i \sin^2(t + \alpha_i)}} -$$

$$\arcsin \frac{\cos A_i}{\sqrt{1 - \sin^2 A_i \sin^2(t + \alpha_i)}},$$

式中： $t=\arcsin \frac{\cos B_i}{\sin A_i}$ 。

由此求得了运动轨迹上相邻两个离散点之间的运动位移量 $(\Delta x_i, \Delta y_i, \Delta z_i, \alpha_i, \beta_i)$ 。

对于上述复杂相贯线接缝自动焊接运动控制算法,利用计算机进行了计算仿真处理,计算结果平滑,拟合出的曲线即为给定的相贯线接缝。

3 伺服运动控制的实现

伺服系统选用基于 PCI 总线的 AC4161 开关量控制卡作为 PC 机控制五个步进电机的通讯接口,硬件结构如图 4 所示。

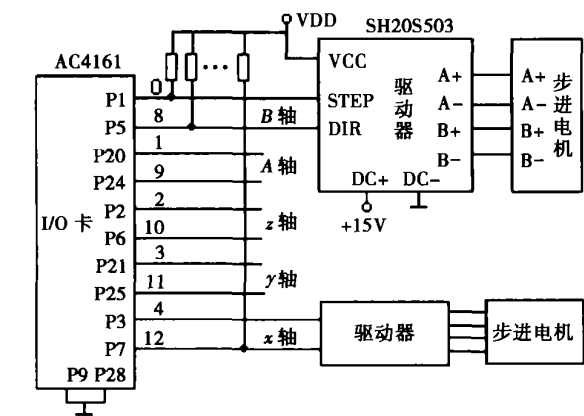


图 4 AC4161 与步进电机驱动器连接示意图
Fig 4 Schematic diagram of AC4161 and stepmotor driver connecting

由上面求得的位移量以及插补周期时间值、各轴脉冲当量或者旋转步距角,自动选择合适的步进电机驱动细分数,可以求取各个步进电机的脉冲数

$N_i(i=x, y, z, A, B)$, 将其存储在相应的数组变量中。在实时焊接时,计算机直接从数组变量中读取各轴步进电机运转的方向与脉冲数,通过 AC4161 向步进电机驱动器输出方向控制信号和步进驱动脉冲,即可驱动各轴步进电机旋转,使焊枪沿着相贯线接缝匀速运动,进而获得给定精度要求的焊缝轨迹。

4 结 论

(1) 通过坐标变换构建相贯线接缝空间曲线方程、利用直线段插补拟合接缝曲线并求取各插补离散点坐标参数与焊枪姿态调整值。

(2) 采用通用开关量控制卡和步进电机组成运动伺服控制系统,执行运动控制算法,实现各轴步进电机的运行脉冲分配,通过五轴电机运动组合完成焊枪、焊件移动控制。该方法降低了硬件配置,增加了系统通用性,同时大大地降低了整台焊接机床的成本。

参考文献:

[1] 杨 箭, 桂贵生. 四坐标自动焊接机床的数控系统[J]. 制造技术与机床, 1997(1): 38—41.
[2] 张忠厚, 李文娟, 刘 强. 锅炉封头相贯线接缝自动焊机的研制[J]. 焊接学报, 1999, 20(12): 114—118.
[3] 张 政, 吴序堂, 马书根, 等. 基于软件化体系结构的数控机床主控系统的开发[J]. 机械工程学报, 2003, 39(2): 93—97.
[4] 王 军, 罗大庸, 黄志辉. 数控焊接机床伺服控制算法的研究[J]. 长沙铁道学院学报, 1998 16(2): 45—48.

作者简介: 霍孟友, 男, 1964 年出生, 工学博士, 副教授。主要研究方向为机电一体化与控制技术, 发表论文 30 余篇。

Email: hmy2618@hotmail.com

MAIN TOPICS, ABSTRACTS & KEY WORDS

Numerical simulation of welding residual stress of tube-to-tubesheet joint in heat exchangers

JIANG Wen-chun, GONG Jian-ming, CHEN Hu, TU Shan-dong (College of Mechanical and Power Engineering, Nanjing University of Technology, Nanjing 210009, China). p1—4

Abstract: Using finite element program-ABAQUS, the welding residual stress of tube-to-tubesheet joint in heat exchangers had been numerically simulated. The distribution of welding residual stress was obtained. A comparison between tube end extended out of tubesheet welded joint and inside hole welded joint was made. The welding residual stress of inside hole welded joint is much smaller than that of tube end extended out of tube sheet joint. So using inside hole welded joint can decrease the susceptibility of stress corrosion cracking (SCC). The maximum of radial stress exists in the HAZ outside surface of tubesheet, which has great influence on tubesheet surface cracks. The maximum of hoop stress appears in the weld root, which has great influence on the connection failure between tube and tubesheet. The residual stress of former pipe bead is decreased due to the later pipe welding heating, which is useful for decreasing the susceptibility of SCC. This work provides a theory reference for optimizing the welding procedure and controlling the welding residual stress for tube-to-tubesheet joint.

Key words: heat exchanger; tube and tubesheet; welding residual stress; finite element ABAQUS

Laser cladded Ni-based alloy coatings reinforced by nano-Sm₂O₃ particles

LI Ming-xi, ZHANG Shi-hong, LI Hui-sheng, HE Yi-zhu (Research Center for Laser Processing, Anhui University of Technology, Maanshan 243002, Anhui, China). p5—8

Abstract: Ni-based alloy coatings with nano/micro-Sm₂O₃ particles addition produced by a 5 kW CO₂ laser on Q235 low carbon steel were introduced. Cross-section of the coatings was examined to reveal their microstructure using optical microscope, scanning electron microscope, and X-ray diffraction instrument. The hardness and wear resistance were measured with microhardness tester and MM200 type sliding wear machine. The results showed that γ -Ni and Cr₂₃C₆ exist in the coatings. Fe₇Sm, Ni₃Si and Ni₃B are also found by adding nano-Sm₂O₃. Fine microstructure and equiaxed dendrite are observed with nano-Sm₂O₃ addition. A thin layer of metallurgical bonding, the white and bright strip, is observed by adding the rare earth oxide. The hardness and wear resistance of the coatings with nano-Sm₂O₃ addition are better than that with micro-Sm₂O₃. The mechanism was found from abrasive/adhesive wear to fretting wear.

Key words: laser cladding; nano-Sm₂O₃; microstructure; microhardness; wear resistance

Movement control algorithm of automatic welding for complex intersection seam

HUO Meng-you, YUE Shao-jian, WANG Xin-gang (School of Mechanical Engineering, Shandong University, Jinan 250061, China). p9—12

Abstract: On the basis of structure and principle of the five-axes linkage NC welding machine introduced in abstract, it mainly studied the movement control algorithm of the automatic welding for the complex intersection seam. Take the ellipsoidal welding conjugation tube as the example, it separately introduced the construction of space curve equation of the intersection seam, the discrete point parameters while interpolating and fitting the intersection seam using line interpolation, the adjusting calculation of welding torch and the method of how to realize the servo control system with digital I/O board and step motor. To control automatic welding process of complex intersection seam using the software algorithm introduced, the system becomes more versatile and the cost of equipment can be decreased considerably.

Key words: automatic welding; intersection line seam; servo-control algorithm

Preliminary discussion about image character of gas pore in MAG welding based on vision sensing

WANG Ke-hong, YOU Qiu-rong, SHEN Ying-ji (Department of Materials, Nanjing University Science & Technology, Nanjing 210094, China). p13—16

Abstract: A passive vision sensing system to acquire the image of molten pool in MAG welding was set up and many typical molten pool images were obtained. The relationship between the typical gas pores and the characteristics of molten pool images were studied by sync contrast experiments. Many molten pool images with surface gas pores and inner gas pores were obtained, and the change of the images and the strange characters were studied from the view of gray mean and gray standard deviation. The experiments indicate that it is feasible to judge the pores by characteristics of the vision images which offers the technological foundation for automatic identification of welding defect on the base of vision sensing. The experiments and the analysis indicate that one type of image may predicate several types of welding defect, one type of welding defect may also shows several types of image characters.

Key words: metal active-gas welding; vision sensing; welding defect; molten pool character

Key techniques of TIG welding robot in high-pressure air condition

XUE Long, WANG Zhong-hui, ZHOU Can-feng, JIAO Xiang-dong (Beijing Institute of Petro-Chemical Technology, Beijing 102617, China). p17—20

Abstract: According to the special technical features of the oil